XL CILAMCE
IBERO-LATIN AMERICAN CONGRESS ON COMPUTATIONAL METHODS IN ENGINEERING
NOVEMBER 11-14, 2019
Praiamar Natal Hotel & Convention
Natal, RN-BRAZIL

# NON-UNIFORM DISPLACEMENT JUMPS IN CELLS WITH EMBEDDED DISCONTINUITY FOR MATERIAL FAILURE ANALYSIS THROUGH THE BOUNDARY ELEMENT METHOD

**Tiago S. Mendonça**
**Rodrigo G. Peixoto**
**Gabriel O. Ribeiro**
*tiagodesouzamendonca@gmail.com*
*rodrigo.peixoto@dees.ufmg.br*
*gabriel@dees.ufmg.br*
*Universidade Federal de Minas Gerais, Departamento de Engenharia de Estruturas*
*Av. Antônio Carlos 6627, 31270-901, Minas Gerais/Belo Horizonte, Brazil*

**Abstract.** The numerical material failures analysis is extremely important, since it allows predicting the collapse and the structures post-critical behavior. Thus, in this work the implicit formulation of the boundary element method is adopted to analyze material failures in models commonly studied in literature. For this purpose, the continuum strong discontinuity approach together with an automatic cell generation algorithm that accompanies the crack trajectory during the non-linear analysis are used. Therefore, the main objective is the insertion of non-uniform jumps discontinuities in the displacement field inside cells aiming at reducing the stress locking phenomenon presented by cells with constant embedded jumps. This phenomenon is responsible for the stiffening in structural response due to the constant cells inability to represent rotation movement. In this way, the results presented by linear cells were more satisfactory than those presented by constant cells, since the stress locking phenomenon was considerably reduced, demonstrating that the first class is more adequate in the representation of the crack opening that occurs during the loading process.

**Keywords:** Linear displacements jumps, Cell with embedded discontinuity, Continuum strong discontinuity approach, Boundary element method

## 1 Introduction

The structural failure analysis has a leading role in engineering, since it makes possible to predict the collapse and the post-critical behaviour of structures subjected to overload. In this sense, we can classify these failures into two types: geometric failures and material failures. Geometric failures are associated with the loss of spatial stability due to the geometrically non-linear behaviour of the structure. On the other hand, material failures are related to the formation of inelastic strain localization bands due to the concentration of micro-structural defects or voids at a material point that progress, as the loading is imposed, until they become visible or macroscopic. This type of failures, in turn, may present different profiles depending on the material type in which they occur, such as shear bands in ductile materials, sliding surfaces in geomechanics or cracks in brittle or quasi-brittle materials. In this way, several numerical techniques were created to analyse such failure types, among which we can highlight: linear elastic fracture mechanics [1–7], discrete or cohesive models [8–12], distributed cracking models [13–17], enriched continuous media [18–20] and the continuum strong discontinuity approach (CSDA) [21–35].

In the CSDA, that was initially introduced by Simo *et al.* [21], it is considered a discontinuous displacement field with the consequent emergence of unlimited strains (the strong discontinuity kinematics) that are consistently applied to standard continuous constitutive models. This process induces a discrete constitutive relation on the discontinuous surface [29, 30]. Another consequence is a regularization of the softening modulus of the continuous constitutive law, resulting from the discontinuous interface equilibrium condition, which establishes that the stress fields should be limited even at points where the strain is not. Thus, the so-called strong discontinuity conditions are obtained which are summarized to a set of kinematic constraint equations necessary for compatibilization between the continuous constitutive model and the strong discontinuity regime.

In many cases, the strong discontinuity surface can be imposed directly at the end of the elastic regime. However, in some materials the formation of the macroscopic crack is preceded by the generation and aggregation of micro-cracks that evolve from a macroscopically continuous state to a discontinuous one. In this way, the fracture process zone has a not negligible size which, in turn, can be divided in three regions: diffuse failure zone, weak discontinuity zone and strong discontinuity zone. In other words, for a better representation of the fracture zone a transient phase should be considered, in weak discontinuity regime, in addition to establishing an efficient procedure to predict the origin and direction of the strain localization band. The weak discontinuity regime is characterized by the presence of jumps in the strain field, however, with the displacement field remaining continuous. A common way to do this is taking the acoustic tensor singularity as a necessary condition for the discontinuous bifurcation of the stress and strain fields [36–38]. In this case, discontinuous bifurcation is characterized by the presence of softening loading within the localization band and the occurrence of elastic unloading, or neutral loading, at the adjacent region.

One of the main steps in the CSDA is the displacement jump field evaluation that is done within the domain discretization elements. Thus, in the context of the finite element method (FEM), it can be shown that finite elements with uniform embedded displacement fields induces the stress locking phenomenon in the structural response when bilinear quadrilateral elements are used. As described in Oliver *et al.* [39], it follows from an incompatibility between the approximation functions for the regular strains (linear) and for the enhanced strains (constant), these last components associated to the displacement jump effects. To overcome this limitation, Manzoli and Shing [40] proposed the insertion of non-uniform embedded discontinuity in quadrilateral finite elements obtaining good results. In this case, the authors considered two collocation points on the discontinuity line in order to obtain linear displacement jumps inside the finite elements.

In the works cited until here, only the standard FEM was adopted in the numerical solution of the problems under study. However, other methods were also employed in the CSDA context. In this sense, we can highlight the works of Oliver *et al.* [41], Belytscho *et al.* [42], Wells and Sluys [43] and Mariani and Perego [44] that employs the generalized (or extended) finite element method (XFEM) and the work

of Manzoli and Venturini [31] that adopt the implicit formulation of the boundary element method (BEM) in fracture analysis of concrete structures. In this last work, the concept of cells with embedded discontinuity was firstly introduced and only triangular cells with uniform (constant) displacement jumps were considered. Also, associative elastoplastic constitutive models with a specific yield criterion, together with an exponential softening law, were used to represent the cracks behaviour. In Manzoli *et al.* [45] the same kind of cells were adopted, however, using an isotropic damage model and a cell generation algorithm to follow the crack path. Besides this, the strong discontinuity regime was imposed directly after the end of the elastic regime with the discontinuity line direction defined as perpendicular to the maximum principal stress. Moreover, in Peixoto *et al.* [32, 33] quadrilateral cells, again with uniform displacement jumps, were used together with another automatic cells generation algorithm. Particularly, in these last works the phases with degradation in continuous media and with weak discontinuities, previously mentioned, were included to a better representation of the fracture process zone. However, as extensively discussed in this paper, despite of the remarkable differences in the strain field evaluations between FEM and BEM, the stress locking phenomenon was also reported for the second technique, suggesting that the consideration of non-uniform displacement jumps inside a cell would be beneficial.

Thus, in the present work cells with two internal collocation points, that permits non-uniform displacement jumps, is presented. Initially, in the linear elastic regime, the cells have, as in all works with BEM cited above, only one collocation point located at their centroid. Subsequently, at the strong discontinuity regime, this point is excluded from the numerical model and two new points are added on the discontinuity line inside the cell. This procedure is numerically translated by eliminating rows and columns to the excluded point and by the addition of new rows and columns for the new points in the appropriate matrices. In this way, these two new points are used in calculating the displacement field jumps through the traction surface continuity condition which, in turn, must be evaluated on the discontinuity line. The consideration of linear jumps inside the cells is justified, as mentioned above, by the emergence of the stress locking phenomenon that occurs in quadrilateral constant cells [32, 33]. The results presented through this new formulation are shown to be satisfactory in reducing such effect showing that non-constant displacement jumps are more appropriate to represent the crack opening movement that occurs during the loading process.

## 2 Integral Equations for Problems with Strong Discontinuities

In this section, the strong discontinuity kinematics and the integral equations for problems with strong discontinuities, used in the BEM, are presented. Besides this, the discontinuous interface equilibrium equation necessary for the displacement jumps evaluation are also presented.

### 2.1 Strong discontinuity kinematics

For the numerical representation of a medium with discontinuities, it is necessary to determine a regularized kinematics capable of distributing the effects of the discontinuous surface in a finite region of the domain [25]. Therefore, we initially define an arbitrary sub-domain $\Omega_\varphi(\subset \Omega)$, around $\mathcal{S}$ as shown through Fig. 1.

Also, it is defined a continuous function $\varphi(\mathbf{X})$, arbitrary in $\Omega_\varphi(\mathbf{X})$, which satisfies the following conditions:

$$\varphi(\mathbf{X}) = \begin{cases} 0, & \text{for } \mathbf{X} \in \Omega^- \backslash \Omega_\varphi^- \\ 1, & \text{for } \mathbf{X} \in \Omega^+ \backslash \Omega_\varphi^+ \end{cases} \tag{1}$$

where the material points are designated by $\mathbf{X}$ and $a \backslash b$ represents $a - (a \cap b)$.

Therefore, one can define the following expression for the regularized displacement rate:

$$\begin{aligned} \dot{u}_i(\mathbf{X},t) &= \underbrace{\dot{\hat{u}}_i(\mathbf{X},t) + \varphi(\mathbf{X})[\![\dot{u}_i]\!](\mathbf{X},t)}_{\dot{\hat{u}}_i(\mathbf{X},t)} + \underbrace{[\mathcal{H}_\mathcal{S}(\mathbf{X}) - \varphi(\mathbf{X})]}_{\mathcal{M}_\mathcal{S}^\varphi(\mathbf{X})}[\![\dot{u}_i]\!](\mathbf{X},t) \\ &= \dot{\hat{u}}_i(\mathbf{X},t) + \mathcal{M}_\mathcal{S}^\varphi(\mathbf{X})[\![\dot{u}_i]\!](\mathbf{X},t) \end{aligned} \tag{2}$$

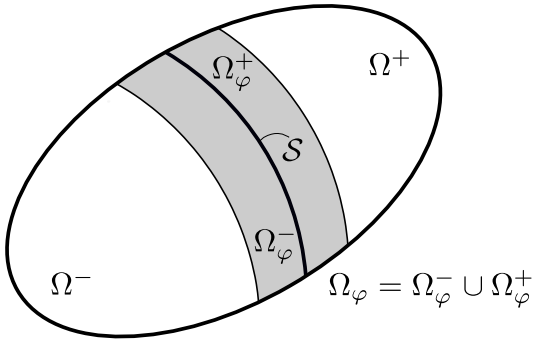


Figure 1. Discontinuous surface contained in an arbitrary subdomain $\Omega_\varphi$

where $\mathcal{H}_\mathcal{S}$ is the Heaviside function ($\mathcal{H}_\mathcal{S} = 1$ for $\mathbf{X} \in \Omega^+$ and $\mathcal{H}_\mathcal{S} = 0$ for $\mathbf{X} \in \Omega^-$) an the terms $\dot{\hat{u}}_i(\mathbf{X}, t)$ and $[\![\dot{u}_i]\!](\mathbf{X}, t)$ represent, respectively, the regular part of the displacement rate field and the displacement rate jump components on the discontinuity surface $\mathcal{S}$. Besides this, $\dot{\hat{u}}_i(\mathbf{X}, t)$ are continuous functions and $\mathcal{M}_\mathcal{S}^\varphi(\mathbf{X})$ has null value for all $\mathbf{X}$ in $\Omega$, except for $\mathbf{X} \in \Omega_\varphi$.

The regularized strain field are given by the symmetric part of the gradient of Eq. (2), that is:

$$\begin{aligned}\dot{\epsilon}_{ij}(\mathbf{X}, t) =& \underbrace{\frac{1}{2}(\dot{\hat{u}}_{i,j} + \dot{\hat{u}}_{j,i})}_{\dot{\hat{\epsilon}}_{ij}} + \underbrace{\frac{\mathcal{M}_\mathcal{S}^\varphi}{2}([\![\dot{u}_{i,j}]\!] + [\![\dot{u}_{j,i}]\!]) - \frac{1}{2}(\varphi_{,i}[\![\dot{u}_j]\!] + \varphi_{,j}[\![\dot{u}_i]\!])}_{-\dot{\epsilon}_{ij}^\varphi} \\ &+ \frac{\delta_\mathcal{S}}{2}([\![\dot{u}_i]\!]n_j + [\![\dot{u}_j]\!]n_i) \\ =& \dot{\hat{\epsilon}}_{ij} - \dot{\epsilon}_{ij}^\varphi + \frac{\delta_\mathcal{S}}{2}([\![\dot{u}_i]\!]n_j + [\![\dot{u}_j]\!]n_i)\end{aligned} \tag{3}$$

where $\dot{\epsilon}_{ij}^\varphi$ has non-zero values only in $\Omega_\varphi$ and the term $\dot{\hat{\epsilon}}_{ij}$ represents the strain field regular portion. Moreover, the term $\delta_\mathcal{S}$ represents the Dirac's line delta function over $\mathcal{S}$ and $n_i$ are the components of the unitary vector normal to the discontinuity surface.

### 2.2 Integral equations with discontinuities

The governing integral equations with discontinuities [32], in the absence of body forces, can be expressed as:

$$\begin{aligned}c_{ij}(\boldsymbol{\xi})\dot{\hat{u}}_j(\boldsymbol{\xi}) =& \int_\Gamma u_{ij}^*(\boldsymbol{\xi}, \mathbf{X})\dot{t}_j(\mathbf{X})d\Gamma(\mathbf{X}) - \fint_\Gamma t_{ij}^*(\boldsymbol{\xi}, \mathbf{X})\dot{\hat{u}}_j(\mathbf{X})d\Gamma(\mathbf{X}) \\ &+ \int_\Omega \sigma_{ijk}^*(\boldsymbol{\xi}, \mathbf{X})\dot{\epsilon}_{jk}^\varphi(\mathbf{X})d\Omega(\mathbf{X})\end{aligned} \tag{4}$$

$$\begin{aligned}\dot{\hat{\epsilon}}_{ij}(\boldsymbol{\xi}) =& \int_\Gamma u_{ijk}^*(\boldsymbol{\xi}, \mathbf{X})\dot{t}_k(\mathbf{X})d\Gamma(\mathbf{X}) - \int_\Gamma t_{ijk}^*(\boldsymbol{\xi}, \mathbf{X})\dot{\hat{u}}_k(\mathbf{X})d\Gamma(\mathbf{X}) \\ &+ \fint_\Omega \sigma_{ijkl}^*(\boldsymbol{\xi}, \mathbf{X})\dot{\epsilon}_{kl}^\varphi(\mathbf{X})d\Omega(\mathbf{X}) + F_{ijkl}^{\epsilon\epsilon}\dot{\epsilon}_{kl}^\varphi(\boldsymbol{\xi})\end{aligned} \tag{5}$$

where Eq. (4) is the displacement boundary integral equation and Eq. (5) is the integral equation for internal strains. In this case, the integral equation for internal displacements (Somigliana's identity) is obtained from Eq. (4) by $c_{ij}(\boldsymbol{\xi}) = 1$ with $\boldsymbol{\xi} \in \Omega$ and $\boldsymbol{\xi} \notin \Gamma$.

In Eqs. (4) and (5) the terms $\hat{u}_i$ and $t_j$ are, respectively, the regular displacements and the tractions on boundary $\Gamma$. Moreover, the tensors $u_{ij}^*(\boldsymbol{\xi}, \mathbf{X})$, $t_{ij}^*(\boldsymbol{\xi}, \mathbf{X})$ and $\sigma_{ijk}^*(\boldsymbol{\xi}, \mathbf{X})$ are the Kelvin's fundamental solutions and represent, respectively, displacements and tractions in the $j$ direction and $jk$ stress components, at a field point $\mathbf{X}$, due to a concentrated unit load at the source point $\boldsymbol{\xi}$ applied in the $i$ direction.

Already the tensors $u^*_{ijk}(\boldsymbol{\xi}, \mathbf{X})$, $t^*_{ijk}(\boldsymbol{\xi}, \mathbf{X})$ and $\sigma^*_{ijkl}(\boldsymbol{\xi}, \mathbf{X})$ represent the Kelvin's fundamental solutions derivatives with respect to the source point $\boldsymbol{\xi}$ and the terms $F^{\epsilon\epsilon}_{ijkl}$ and $c_{ij}(\boldsymbol{\xi})$ are free terms associated with particular analytical integrations. It is also worth to mention that the first and third integrals on the right side the Eq. (4) have weak singularities and the second integral on the right side of the same equation together with the third integral on the right side of the Eq. (5) have strong singularities when $\boldsymbol{\xi}$ and $\mathbf{X}$ coincide. In these cases, special integration techniques need to be used. In this work, the methodologies adopted can be seen in Lachat and Watson [46] and Gao and Davies [47] in the evaluation of the weak and strong singularities, respectively. The remaining integrals do not have any singularity and can, therefore, be integrated by conventional gauss quadrature.

### 2.3 Equilibrium equation of the discontinuous interface

Equations (4) and (5) do not completely define the boundary value problem, since the internal continuity condition of the surface forces is not met [32, 33]. Therefore, the interface equilibrium equation must also be satisfied:

$$f_i = \left\{ E^o_{ijkl}\left[\hat{\epsilon}_{kl} - \epsilon^{\varphi}_{kl}([\![u_i]\!], [\![u_{i,j}]\!])\right] - \sigma^{\mathcal{S}}_{ij}(\epsilon_{ij}) \right\} n_j = 0 \tag{6}$$

In this equation $\epsilon_{ij}$ is given by the time integration of Eq. (3) which, for points on $\mathcal{S}$, corresponds to the following expression:

$$\epsilon_{ij} = \hat{\epsilon}_{ij} - \epsilon^{\varphi}_{ij} + \frac{1}{2h}([\![u_i]\!] n_j + [\![u_j]\!] n_i); \quad h \longrightarrow 0 \tag{7}$$

In the context of the boundary element method, Eq. (6) can be solved numerically by the adoption of cells with embedded discontinuities that provide the displacement jump components ($[\![u_i]\!]$) required to evaluate $\epsilon^{\varphi}_{ij}$. These components are considered linear inside the cells and are obtained through the adoption of two collocation points in opposition to the previous works with BEM in which only uniform jump components have been used inside a cell. In this way, considering a given regular strain $\hat{\epsilon}_{ij}$ for each collocation point, and taking into account Eq. (7), we have that Eq. (6) can be written as $f_i \equiv f_i([\![u_i]\!], [\![u_{i,j}]\!] = 0$. Therefore, after linearization of this equation, its solution can be obtained through Newton's method.

From these considerations, a regularized constitutive equation that relates stresses and regular strains ($\hat{\epsilon}_{ij}$) can be defined, that is:

$$\tilde{\sigma}_{ij}(\hat{\epsilon}_{ij}) = \sigma^{\Omega\setminus\mathcal{S}}_{ij}\Big(\hat{\epsilon}_{ij} - \epsilon^{\varphi}_{ij}\big([\![u_i]\!](\hat{\epsilon}_{ij}), [\![u_{i,j}]\!](\hat{\epsilon}_{ij})\big)\Big) = E^o_{ijkl}(\hat{\epsilon}_{kl} - \epsilon^{\varphi}_{kl}) \tag{8}$$

where $[\![u_i]\!](\hat{\epsilon}_{ij})$ and its gradient, $[\![u_{i,j}]\!](\hat{\epsilon}_{ij})$, comes from solution of Eq. (6).

## 3 Implicit Formulation of the BEM for Problems with Discontinuities

After BEM standard discretization, Eqs. (4) and (5) can be rewritten in matrix form as [32, 33]:

$$[H]\{\dot{\hat{u}}\} = [G]\{\dot{t}\} + [Q_{\epsilon^{\varphi}}]\{\dot{\epsilon}^{\varphi}\} \tag{9}$$

$$\{\dot{\hat{\epsilon}}\} = [G^{\epsilon}]\{\dot{t}\} - [H^{\epsilon}]\{\dot{\hat{u}}\} + [Q^{\epsilon}_{\epsilon^{\varphi}}]\{\dot{\epsilon}^{\varphi}\} \tag{10}$$

where matrix $[H]$ is composed by the free terms ($c_{ij}$) and the terms from the second integral on the right hand side of Eq. (4). Already the matrices $[G]$ and $[Q_{\epsilon^{\varphi}}]$ are composed by the terms from the first and third integrals on the right hand side of this same equation. With respect to matrices in Eq. (10) we have that $[G^{\epsilon}]$ and $[H^{\epsilon}]$ are composed by the terms in the first and second integrals in the right hand side of Eq. (5), respectively, and $[Q^{\epsilon}_{\epsilon^{\varphi}}]$ is formed by the third integral and the last term in the right hand side of this same equation.

Applying the essential and natural boundary conditions, the Eqs. (9) and (10) can be re-arranged as:

$$[A]\{\dot{x}\} = [B]\{\dot{y}\} + [Q_{\epsilon^\varphi}]\{\dot{\epsilon}^\varphi\} \tag{11}$$

$$\{\dot{\hat{\epsilon}}\} = [A^\epsilon]\{\dot{x}\} + [B^\epsilon]\{\dot{y}\} + [Q^\epsilon_{\epsilon^\varphi}]\{\dot{\epsilon}^\varphi\} \tag{12}$$

where the matrices $[A]$ and $[B]$ are composed by the coefficients from the matrices $[H]$ and $[G]$ and the matrices $[A^\epsilon]$ and $[B^\epsilon]$ are composed by the coefficients from the matrices $[H^\epsilon]$ and $[G^\epsilon]$. In vectors $\{\dot{y}\}$ and $\{\dot{x}\}$ are grouped, respectively, the prescribed and the unknown values of the boundary stemming from $\{\dot{u}\}$ or $\{\dot{t}\}$.

From Eq. (11), we find:

$$\{\dot{x}\} = [N]\{\dot{y}\} + [M_{\epsilon^\varphi}]\{\dot{\epsilon}^\varphi\} \tag{13}$$

where:

$$[N] = [A]^{-1}[B], \quad [M_{\epsilon^\varphi}] = [A]^{-1}[Q_{\epsilon^\varphi}] \tag{14}$$

Now replacing Eq. (13) in (12), it is found:

$$\{\dot{\hat{\epsilon}}\} = [N^\epsilon]\{\dot{y}\} + [M^\epsilon_{\epsilon^\varphi}]\{\dot{\epsilon}^\varphi\} \tag{15}$$

being that:

$$[N^\epsilon] = [A^\epsilon][A]^{-1}[B] + [B^\epsilon], \quad [M^\epsilon_{\epsilon^\varphi}] = [A^\epsilon][A]^{-1}[Q_{\epsilon^\varphi}] + [Q^\epsilon_{\epsilon^\varphi}] \tag{16}$$

The constitutive model considered in this work is a rate independent model, in such a way that time derivatives can be substituted by finite increments, i.e.,

$$\{\hat{\epsilon}\}^i = \lambda^i[N^\epsilon]\{y\} + [M^\epsilon_{\epsilon^\varphi}]\{\epsilon^\varphi\}^i \tag{17}$$

being that, $\dot{(\cdot)} = (\cdot)_i - (\cdot)_{i-1}$, where $i$ is an incremental index. In addition, $\lambda^i$ is a cumulative scalar value called load factor and whose evolution depends on a specific control method [48].

From Eq. (17), we can now define an equilibrium vector, $\{Q\}^i \equiv \{Q(\hat{\epsilon}^i, \lambda^i)\}$, as a function of the regular strains and the load factor, that is:

$$\{Q\}^i = \lambda^i[N^\epsilon]\{y\} + [M^\epsilon_{\epsilon^\varphi}]\big(\{\hat{\epsilon}\}^i - [E^o]^{-1}\{\tilde{\sigma}(\hat{\epsilon})\}^i\big) - \{\hat{\epsilon}\}^i = \{0\} \tag{18}$$

where it was taken into account the matrix form of the regularized constitutive equation (Eq. 8) applied to the complete set of internal cells. In addition, in Eq. (18) the term $[E^o]$ now represents the linear elastic quasi-diagonal matrix.

Equation (18) in then linearized and solved by Newton's method in each load increment. The complete algorithm can be seen in Peixoto *et al.* [33].

## 4 Isotropic Damage Constitutive Model

In the numerical analyses performed in this work, an isotropic damage constitutive model is used. This model can be synthesized through the following equations [32]:

$$\psi(\epsilon_{ij}, r) = [1 - D(r)]\psi_o(\epsilon_{ij}), \quad \psi_o(\epsilon_{ij}) = \frac{1}{2}\epsilon_{ij}E^o_{ijkl}\epsilon_{kl} \tag{19}$$

$$\sigma_{ij} = \frac{\partial\psi(\epsilon_{ij}, r)}{\partial\epsilon_{ij}} = (1 - D)E^o_{ijkl}\epsilon_{kl} = E_{ijkl}\epsilon_{kl} \tag{20}$$

$$D \equiv D(r) = 1 - \frac{q(r)}{r}, \quad D \in [0, 1] \tag{21}$$

$$\dot{r} = \dot{\gamma}, \quad \begin{cases} r \in [r_o, \infty), \\ r_o = r|_{t=0} = \frac{f_t}{\sqrt{E}} \end{cases} \tag{22}$$

$$\bar{F}(\epsilon_{ij}, r) = \tau_\epsilon - r \tag{23}$$

$$\bar{F} \leqslant 0, \quad \dot{\gamma} \geqslant 0, \quad \dot{\gamma}\bar{F} = 0, \quad \dot{\gamma}\dot{\bar{F}} = 0 \tag{24}$$

$$\dot{q} = H(r)\dot{r}, \quad (H = q'(r) \leqslant 0), \quad \begin{cases} q \in [0, r_o], \\ q|_{t=0} = r_o \end{cases} \tag{25}$$

Equation (19) represents the expression for Helmholtz free energy. In this equation the term $r$ is the strain-like scalar internal variable. In addition, $D$ is the damage variable and $E^o_{ijkl}$ represents the elastic constitutive tensor for isotropic materials which is given by:

$$E^o_{ijkl} = \bar{\lambda}\delta_{ij}\delta_{kl} + \mu(\delta_{ik}\delta_{jl} + \delta_{il}\delta_{jk}) \tag{26}$$

where $\delta_{ij}$ is the Kronecker delta and the terms $\mu$ and $\bar{\lambda}$ represent the Lamé constants that are expressed as:

$$\mu = \frac{E}{2(1+\nu)}; \quad \bar{\lambda} = \frac{2\mu\bar{\nu}}{1-2\bar{\nu}} \tag{27}$$

where $E$ is the elasticity modulus, $\nu$ is the Poisson's ratio and $\bar{\nu}$ is given by:

$$\bar{\nu} = \begin{cases} \nu, & \text{for 3D and plane strain state} \\ \dfrac{\nu}{1+\nu}, & \text{for plane stress state} \end{cases} \tag{28}$$

Already Eqs. (20) to (25) represent, respectively, a constitutive equation, an expression for the damage variable, the evolution law of the internal variable, a damage criterion, the Kuhn-Tucker conditions and a softening law. In these expressions, the term $\sigma_{ij}$ represents the Cauchy stress tensor, $E_{ijkl}$ represents the secant tensor of the constitutive relation, $q$ is the stress-like internal scalar variable, $f_t$ refers to the material tensile strength, $\bar{F}$ represents the damage function in the strain space, $\tau_\epsilon$ is the equivalent strain and $H$ is the hardening-softening modulus.

Different damage criteria can be obtained from the choice of the $\tau_\epsilon$ parameter (Eq. 23). In this work, the same damage criterion used by Oliver *et al.* [49] is adopted, that is:

$$\tau_\epsilon = \sqrt{\epsilon^+_{ij} E^o_{ijkl} \epsilon_{kl}} \tag{29}$$

In Eq. (29) the tensor $\epsilon^+_{ij}$ is defined, taking into account a coordinate system aligned with the strain principal directions, such as:

$$\epsilon^+_{ij} = \sum_{k=1}^{n_{dim}} \langle \epsilon_k \rangle \hat{\mathbf{e}}_k \otimes \hat{\mathbf{e}}_k \tag{30}$$

where the term $\epsilon_k$ represents the $k$-th principal strain, $\hat{\mathbf{e}}_k$ represents a unit vector in the corresponding principal direction and $\langle \epsilon_k \rangle = (|\epsilon_k| + \epsilon_k)/2$. Thus, this model becomes suitable for the representation of quasi-brittle materials, since the degradation will occur in traction states preferentially.

An incremental constitutive equation can be obtained from Eq. (20) considering the inelastic loading condition ($\dot{r} = \dot{\tau}_\epsilon$), that is:

$$\begin{aligned} \dot{\sigma}_{ij} &= (1-D)E^o_{ijkl}\dot{\epsilon}_{kl} - \dot{D}E^o_{ijkl}\epsilon_{kl} \\ &= E_{ijkl}\dot{\epsilon}_{kl} - \left(\frac{\partial D}{\partial r}\right)\dot{r}E^o_{ijkl}\epsilon_{kl} \\ &= \left[E_{ijkl} - \left(\frac{\partial D}{\partial r}\right)\left(\frac{\partial \tau_\epsilon}{\partial \epsilon_{kl}}\right)E^o_{ijrs}\epsilon_{rs}\right]\dot{\epsilon}_{kl} \\ &= E^t_{ijkl}\dot{\epsilon}_{kl} \end{aligned} \tag{31}$$

where $E^t_{ijkl}$ is the tangent operator of the constitutive model.

For the strong discontinuity regime an exponential softening law, that compatibilizes the continuous constitutive model with the strong discontinuity kinematics [32, 45], is adopted for Eq. (25), that is:

$$q(r) = r_o e^{\frac{r_o^2 h}{G_f}\left(1-\frac{r}{r_o}\right)} \tag{32}$$

where $G_f$ represents the fracture energy.

From Eqs. (21) and (32) we find the following expression for the damage variable evolution:

$$D(r) = 1 - \frac{r_o}{r} e^{\frac{r_o^2 h}{G_f}\left(1-\frac{r}{r_o}\right)} \quad \text{for} \quad r > r_o \tag{33}$$

## 5 Cells with non-uniform embedded discontinuity

In this section we describe the new class of cells with embedded strong discontinuity that is developed through this work. These cells present non-uniform displacement jumps in their interior and until the present moment have not yet been studied. Although the focus of this section is on the description of cells with non-uniform displacement jumps, the methodology used here is easily extended to cells with higher approximation orders for the displacement jumps, thus contributing to a generalization of the concept of cells with embedded strong discontinuity.

### 5.1 Description of a cell with linear displacement jump

From the definition of the function $\varphi(\mathbf{X})$ (Eq. 1), we can see that the dissipative effects are restricted to the subdomain $\Omega_\varphi$. Therefore, only this region needs to be discretized by cells, as illustrated by Fig. 2a.

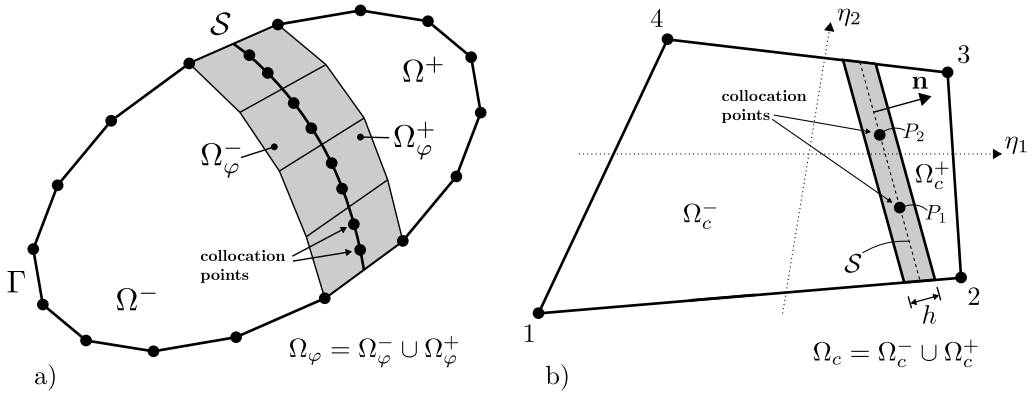


Figure 2. BEM discretization of a solid with discontinuity surface: a) Boundary and domain discretization, b) Cell with embedded discontinuity

In this work, the strong discontinuity regime is directly imposed at the end of the elastic regime. Thus, as previously mentioned in Section 1, before the inelastic behaviour the cells have only one collocation point at their centroid. Subsequently, in the strong discontinuity regime, this collocation point is excluded from the numerical model and two other points are created along the discontinuity line, as illustrated in Fig. (2b). This process is more detailed in Section 6.

The displacement jumps inside the cells are obtained through the numerical solution of the interface equilibrium equation (Eq. 6). In this way, it is considered that the displacement jumps have a linear variation inside a cell which are approximated through the following expression:

$$[\![u_i]\!](\bar{\xi}) \approx N_1(\bar{\xi})[\![u_i]\!]^1 + N_2(\bar{\xi})[\![u_i]\!]^2 \tag{34}$$

where $[\![u_i]\!]^1$ and $[\![u_i]\!]^2$ represent the displacement jumps at collocation points $P_1$ and $P_2$, respectively (see Fig. 3).

Therefore, based on Eq. (34), we have:

$$\begin{Bmatrix} [\![u_1]\!](\bar{\xi}) \\ [\![u_2]\!](\bar{\xi}) \end{Bmatrix} \approx \begin{bmatrix} N_1(\bar{\xi}) & 0 & N_2(\bar{\xi}) & 0 \\ 0 & N_1(\bar{\xi}) & 0 & N_2(\bar{\xi}) \end{bmatrix} \begin{Bmatrix} [\![u_1]\!]^1 \\ [\![u_2]\!]^1 \\ [\![u_1]\!]^2 \\ [\![u_2]\!]^2 \end{Bmatrix} \tag{35}$$

In Eqs. (34) and (35) the terms $N_1$ and $N_2$ are interpolation functions such that:

$$N_1 = (1 - \bar{\xi})/2; \qquad N_2 = (1 + \bar{\xi})/2; \tag{36}$$

where the term $\bar{\xi}$ represents a dimensionless coordinate axis defined along the discontinuity line (Fig. 3) which can be expressed as:

$$\bar{\xi}(x, y) = ax + by + c; \tag{37}$$

The parameters $a$, $b$ and $c$ in Eq. (37) are constant scalars, obtained through the following conditions:

$$\bar{\xi}(x_1, y_1) = -1; \qquad \bar{\xi}(x_2, y_2) = +1; \qquad \bar{\xi}(x_n, y_n) = -1; \tag{38}$$

where $(x_1, y_1)$ and $(x_2, y_2)$ represent the coordinates of the collocation points $P_1$ and $P_2$, respectively, and $(x_n, y_n)$ represents the coordinates of a fictitious point, $P_N$, whose orthogonal distance to the collocation point 1 is equal to one unit. This scheme is shown in Fig. 3.

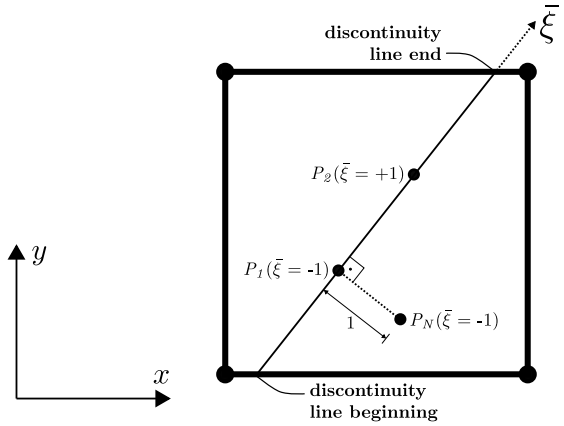


Figure 3. Conditions for defining the coordinates transformation $\bar{\xi}(x, y)$

In addition, for the strong discontinuity regime, the field $\epsilon_{ij}^{\varphi}$ is considered linear through the following expression:

$$\{\epsilon^{\varphi}\} = N_1\{\epsilon^{\varphi,1}\} + N_2\{\epsilon^{\varphi,2}\} \tag{39}$$

where the terms $\{\epsilon^{\varphi,1}\}$ and $\{\epsilon^{\varphi,2}\}$ represent the initial fields at collocation points $P_1$ and $P_2$, respectively.

The cell geometry is parametrized by conventional linear shape functions $M^{\alpha}(\eta_1, \eta_2)$ defined by the natural coordinates $\eta_i$, that is:

$$X_j(\eta_1, \eta_2) \approx M^{\alpha}(\eta_1, \eta_2) X_j^{\alpha} \tag{40}$$

where the $\alpha$ index refers to the corner points (numbered from 1 to 4 in Fig. 2b).

Therefore, in a non-constant cell with embedded discontinuity, a set of internal collocation points and a set of geometric interpolation points can be distinguished. In addition, the discontinuity line orientation is defined by its unit normal vector, $n_i$, and a very small value parameter, $h$ (see Eq. 7), is used to regularize the Dirac delta function.

The geometry interpolation functions can also be used to define the function $\varphi(\mathbf{X})$ inside the cell since the conditions, $\varphi(\mathbf{X}) = 0$ in $\Omega^- \backslash \Omega_{\varphi}^-$ and $\varphi(\mathbf{X}) = 1$ in $\Omega^+ \backslash \Omega_{\varphi}^+$, are satisfied by the choice:

$$\varphi(\mathbf{X}(\eta_1, \eta_2)) = \sum_{\alpha^+} M^{\alpha^+}(\eta_1, \eta_2) \tag{41}$$

In this case, the summation is performed considering the interpolation functions associated with the corners located in $\Omega_c^+$ (e.g., points 2 and 3 in Fig. 2b).

### 5.2 Evaluation of displacement jumps

From Eq. (3), the vector $\{\epsilon^{\varphi}\}$ in a collocation point inside a cell may be written as:

$$\{\epsilon^{\varphi}\} = \begin{Bmatrix} \epsilon_{11}^{\varphi} \\ \epsilon_{22}^{\varphi} \\ \epsilon_{12}^{\varphi} \end{Bmatrix} = \begin{bmatrix} \varphi,_1 & 0 \\ 0 & \varphi,_2 \\ \frac{1}{2}\varphi,_2 & \frac{1}{2}\varphi,_1 \end{bmatrix} \begin{Bmatrix} [\![u_1]\!] \\ [\![u_2]\!] \end{Bmatrix} - \mathcal{M}_{\mathcal{S}}^{\varphi} \begin{Bmatrix} [\![u_{1,1}]\!] \\ [\![u_{2,2}]\!] \\ \frac{1}{2}[\![u_{1,2}]\!] + \frac{1}{2}[\![u_{2,1}]\!] \end{Bmatrix} \tag{42}$$

where, from Eqs. (40) and (41), we have that:

$$\varphi,_i = \frac{\partial \varphi}{\partial \eta_k}\frac{\partial \eta_k}{\partial X_i} = \left(\frac{\partial M^{\alpha}}{\partial \eta_k} X_i^{\alpha}\right)^{-1} \left(\frac{\partial}{\partial \eta_k}\left[\sum_{\alpha^+} M^{\alpha^+}\right]\right) \tag{43}$$

Thus, considering Eq. (35) and the gradient of the linear displacement jumps, we can rewrite Eq. (42) as:

$$\begin{aligned} \{\epsilon^{\varphi}\} = \begin{Bmatrix} \epsilon_{11}^{\varphi} \\ \epsilon_{22}^{\varphi} \\ \epsilon_{12}^{\varphi} \end{Bmatrix} &= \begin{bmatrix} \varphi,_1 & 0 \\ 0 & \varphi,_2 \\ \frac{1}{2}\varphi,_2 & \frac{1}{2}\varphi,_1 \end{bmatrix} \begin{bmatrix} N_1(\xi) & 0 & N_2(\xi) & 0 \\ 0 & N_1(\xi) & 0 & N_2(\xi) \end{bmatrix} \begin{Bmatrix} [\![u_1]\!]^1 \\ [\![u_2]\!]^1 \\ [\![u_1]\!]^2 \\ [\![u_2]\!]^2 \end{Bmatrix} - \mathcal{M}_{\mathcal{S}}^{\varphi} \begin{bmatrix} -\frac{1}{2}a & 0 & \frac{1}{2}a & 0 \\ 0 & -\frac{1}{2}b & 0 & \frac{1}{2}b \\ -\frac{1}{4}b & -\frac{1}{4}a & \frac{1}{2}b & \frac{1}{4}a \end{bmatrix} \begin{Bmatrix} [\![u_1]\!]^1 \\ [\![u_2]\!]^1 \\ [\![u_1]\!]^2 \\ [\![u_2]\!]^2 \end{Bmatrix} \\ &= [\nabla^s \varphi][N]\{[\![u]\!]\} - \mathcal{M}_{\mathcal{S}}^{\varphi}[\bar{J}]\{[\![u]\!]\} \\ &= \Big([\nabla^s \varphi][N] - \mathcal{M}_{\mathcal{S}}^{\varphi}[\bar{J}]\Big)\{[\![u]\!]\} \end{aligned} \tag{44}$$

Besides this, considering Eqs. (7) and (44), we find the following expression for the interface equilibrium equation (Eq. 6), for each collocation point inside a cell:

$$\begin{aligned} \{f_k\} = [\bar{N}^c]^T \big([E^o]\{\hat{\epsilon}^k\} - [E^o]\Big[[\nabla^s \varphi][N] - \mathcal{M}_{\mathcal{S}}^{\varphi}[\bar{J}]\Big]\{[\![u]\!]\} \\ - \{\sigma_k^{\mathcal{S}}(\{\hat{\epsilon}^k\} - \Big[[\nabla^s \varphi][N] - \mathcal{M}_{\mathcal{S}}^{\varphi}[\bar{J}]\Big]\{[\![u]\!]\} + \frac{1}{h}[N^c][N]\{[\![u]\!]\})\} = \{0\} \end{aligned} \tag{45}$$

where $k = 1, 2$ and:

$$[\bar{N}^c] = \begin{bmatrix} n_1 & 0 \\ 0 & n_2 \\ n_2 & n_1 \end{bmatrix}; \quad [N^c] = \begin{bmatrix} n_1 & 0 \\ 0 & n_2 \\ \frac{1}{2}n_2 & \frac{1}{2}n_1 \end{bmatrix} \tag{46}$$

Now, for a given regular strain state in each collocation point, $\{\hat{\epsilon}^k\}$, Eq. (45) can then be solved by Newton's method after its linearization, i.e.,

$$\{f_k\}_{j-1} + \left[\frac{\partial \{f_k\}}{\partial \{[\![u]\!]\}}\right]_{j-1} \{\delta[\![u]\!]\}_j \approx 0 \tag{47}$$

where $j$ is an iterative index, $\{\delta[\![u]\!]\}_j = \{[\![u]\!]\}_j - \{[\![u]\!]\}_{j-1}$, and:

$$\begin{aligned} \left[\frac{\partial \{f_k\}}{\partial \{[\![u]\!]\}}\right]_{j-1} = [\bar{N}^c]^T \Bigg\{ &- [E^o]\Big([\nabla^s \varphi][N] - \mathcal{M}_{\mathcal{S}}^{\varphi}[\bar{J}]\Big) \\ &- \left[\frac{\partial \sigma^{\mathcal{S}}}{\partial \epsilon}\right]_{j-1} \Big[ - [\nabla^s \varphi][N] + \mathcal{M}_{\mathcal{S}}^{\varphi}[\bar{J}] + \frac{1}{h}[N^c][N]\Big] \Bigg\} \end{aligned} \tag{48}$$

where the term $\left[\frac{\partial \sigma^{\mathcal{S}}}{\partial \epsilon}\right]$ is the tangent operator of the continuous constitutive model, presented in Eq. (31), used to represent the dissipative effects on the discontinuity line $\mathcal{S}$.

Therefore, Eqs. (45), (47) and (48) are applied simultaneously to the two collocation points located on the cell's discontinuity line generating a $4 \times 4$ equation system, that is:

$$\begin{Bmatrix} f_1 \\ f_2 \end{Bmatrix}_{j-1} + \begin{bmatrix} \left[\frac{\partial\{f_1\}}{\partial\{[\![u]\!]\}}\right] \\ \left[\frac{\partial\{f_2\}}{\partial\{[\![u]\!]\}}\right] \end{bmatrix}_{j-1} \begin{Bmatrix} \delta[\![u_1]\!]^1 \\ \delta[\![u_2]\!]^1 \\ \delta[\![u_1]\!]^2 \\ \delta[\![u_2]\!]^2 \end{Bmatrix}_{j} \approx \begin{Bmatrix} 0 \\ 0 \\ 0 \\ 0 \end{Bmatrix} \tag{49}$$

Thus, once Eq. (49) is solved by Newton's iterative method, the components of the displacement jumps inside the cells with embedded discontinuity are obtained.

### 5.3 Regularized constitutive model and its tangent operator

Based on the formulation presented above, the regularized constitutive relation of Eq. (8) assumes the next form for an individual collocation point inside a cell:

$$\begin{aligned} \{\tilde{\sigma}(\hat{\epsilon}^k)\} =& [E^o](\{\hat{\epsilon}^k\} - \{\epsilon^{\varphi,k}\}) \\ =& [E^o]\Big[\{\hat{\epsilon}^k\} - \Big([\nabla^s \varphi][N(\bar{\xi}^k)] - \mathcal{M}^{\varphi}_{\mathcal{S}}[\bar{J}]\Big)\{[\![u]\!]\}\Big] \end{aligned} \tag{50}$$

In addition, the non-linear solution strategy requires a tangent operator from this regularized constitutive equation, which can be done by taking the derivative:

$$\begin{aligned} \left[\frac{\partial \tilde{\sigma}}{\partial \hat{\epsilon}^k}\right] &= [E^o]\left([I] - \left[\frac{\partial\{\epsilon^{\varphi}\}}{\partial\{\hat{\epsilon}^k\}}\right]\right) \\ &= [E^o]\Bigg([I] - \underbrace{\left[\frac{\partial\{\epsilon^{\varphi}\}}{\partial\{[\![u]\!]\}}\right]}_{1st\text{ term}} \underbrace{\left[\frac{\partial\{f_k\}}{\partial\{[\![u]\!]\}}\right]^{-1}}_{2st\text{ term}} \underbrace{\left[\frac{\partial\{f\}}{\partial\{\hat{\epsilon}^k\}}\right]}_{3st\text{ term}}\Bigg) \end{aligned} \tag{51}$$

The first term highlighted in Eq. (51) can be expressed as:

$$\left[\frac{\partial\{\epsilon^{\varphi}\}}{\partial\{[\![u]\!]\}}\right] = \Big([\nabla^s \varphi][N(\bar{\xi}^k)] - \mathcal{M}^{\varphi}_{\mathcal{S}}[\bar{J}]\Big) \tag{52}$$

where Eq. (44) has been taken into account.

The second term is obtained by employing the pseudo-inverse concept [50], since $\left[\frac{\partial\{f_k\}}{\partial\{[\![u]\!]\}}\right]$ is a non-square matrix. In this way, one has to:

$$\left[\frac{\partial\{f_k\}}{\partial\{[\![u]\!]\}}\right]^{-1} = \left[\frac{\partial\{f_k\}}{\partial\{[\![u]\!]\}}\right]^{T} \left(\left[\frac{\partial\{f_k\}}{\partial\{[\![u]\!]\}}\right]\left[\frac{\partial\{f_k\}}{\partial\{[\![u]\!]\}}\right]^{T}\right)^{-1} \tag{53}$$

Finally, the third and last term, in turn, is obtained from Eq. (45), i.e.,

$$\left[\frac{\partial\{f_k\}}{\partial\{\hat{\epsilon}^k\}}\right] = [\bar{N}^c]^T \left([E^o] - \left[\frac{\partial\{\sigma^{\mathcal{S}}_k\}}{\partial\{\hat{\epsilon}^k\}}\right]\right) \tag{54}$$

## 6 Discontinuity line tracking algorithm

The discontinuous line is propagated along the solid domain through an automatic cell generation algorithm according to the scheme shown in Fig. 4.

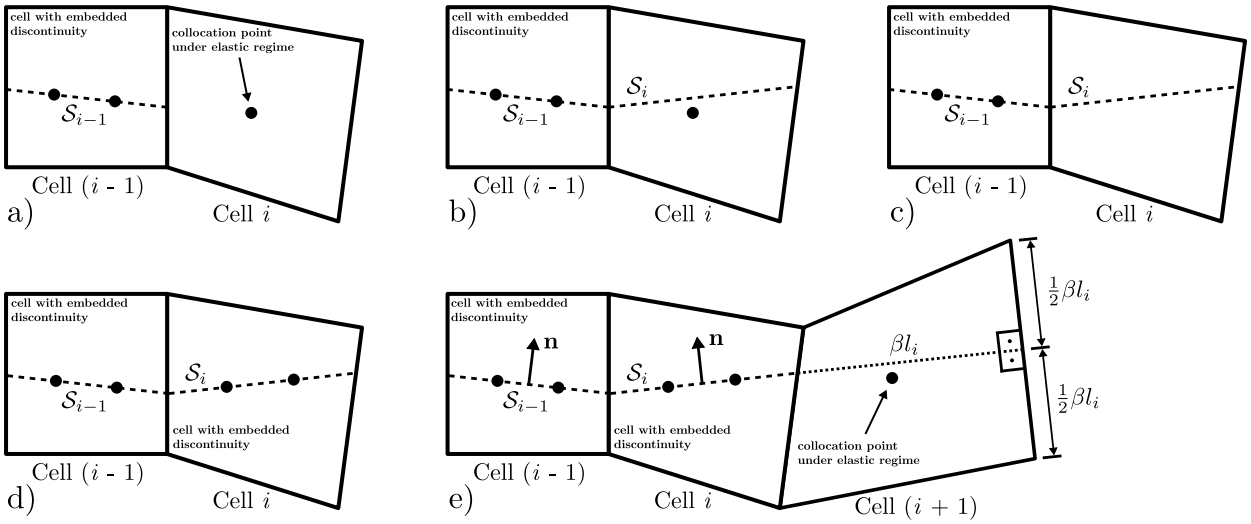


Figure 4. Automatic cell generation algorithm: a) Cell $i$ under elastic regime, b) Tracing of the discontinuity line in cell $i$, c) Elimination of the collocation point in cell $i$, d) Insertion of 2 new collocation points in cell $i$, e) Generation of a new cell in elastic regime (cell $(i + 1)$)

In front of the last cell in strong discontinuity regime (Cell $(i - 1)$ in Fig. 4a) there is always a cell in elastic regime (Cell $i$ also in Fig. 4a). When the elastic limit is reached, a straight discontinuity segment is introduced, perpendicularly to the maximum principal stress direction (Fig. 4b), ensuring discontinuous line continuity (lines $\mathcal{S}_{i-1}$ and $\mathcal{S}_i$). Then, the collocation point located in the centroid of the cell $i$ is excluded from the numerical model (Fig. 4c) and other two collocation points are inserted over the discontinuity line (Fig. 4d). In this case, the points are inserted at a distance of $1/3$ and $2/3$ of the discontinuity line length. Finally, with reference to the Fig. 4e, a new cell (Cell $(i + 1)$) is generated from the following steps:

i. The edge of the cell $i$ that contains the end of the discontinuity line is assumed to be the starting edge of the cell $(i + 1)$;
ii. A straight segment is drawn from the end point of the discontinuity segment of the previous cell following the same orientation as this, but with length weighted by a scalar factor, $\beta$;
iii. The opposite side of the new cell is created perpendicularly to this segment, with its same size and taking its final point as the side's midpoint;
iv. The other two sides of the new cell are created by connecting the endpoints of these first two sides.

In this case, the use of $\beta$ parameter becomes important in some cases to prevent the occurrence of numerical instabilities and for the reduction of numerical processing time [51].

## 7 Numerical Examples

In the numerical analyses carried out in this work, the isotropic damage constitutive model described in Section 4 is adopted to represent the dissipative affects over the discontinuity line. The strong discontinuity regime is imposed directly at the end of the elastic regime assuming $h = 0.01$ mm in Eqs. (32) and (33). Besides this, the discontinuity segment orientation inside the cell was adopted as perpendicular to the maximum principal stress direction. For the non-linear analysis, a tolerance of $1 \times 10^{-4}$ was considered with the cells generation occurring (if necessary) only after a step convergence.

### 7.1 Example 1: Bending Test

The first example analyzed is a simple bending test. A schematic drawing of such test is shown through Fig. 5, where the geometry, loads and the material properties are also presented.

The discontinuity line was pre-fixed at the center of the cell with embedded discontinuity. This cell

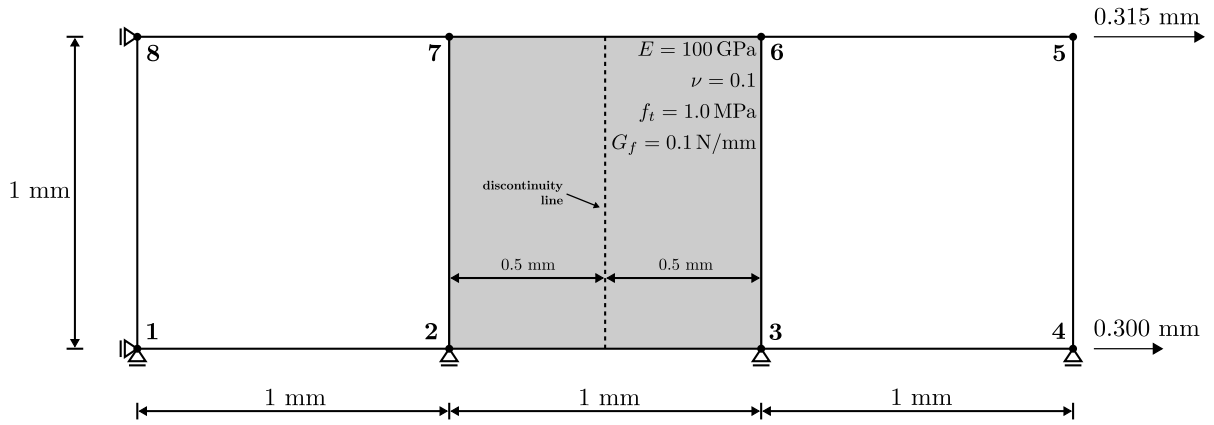


Figure 5. Example 1: Simple bending test

is represented by the dark gray area in Fig. 5. In addition, 8 linear elements are employed in the boundary discretization. Prescribed displacements of 0.300 mm and 0.315 mm were imposed on collocation points 4 and 5, respectively, and analyzes were performed considering a cell with 1 collocation point, i.e., with uniform displacement jumps components as in the works of Peixoto *et al.* [32, 33], and the cell developed in this work with 2 collocation points, i.e., with non-uniform displacement jumps components. The horizontal traction obtained for the collocation points 4 and 5 were plotted in function of point 4 displacement. The results are shown in Figs. 6 and 7.

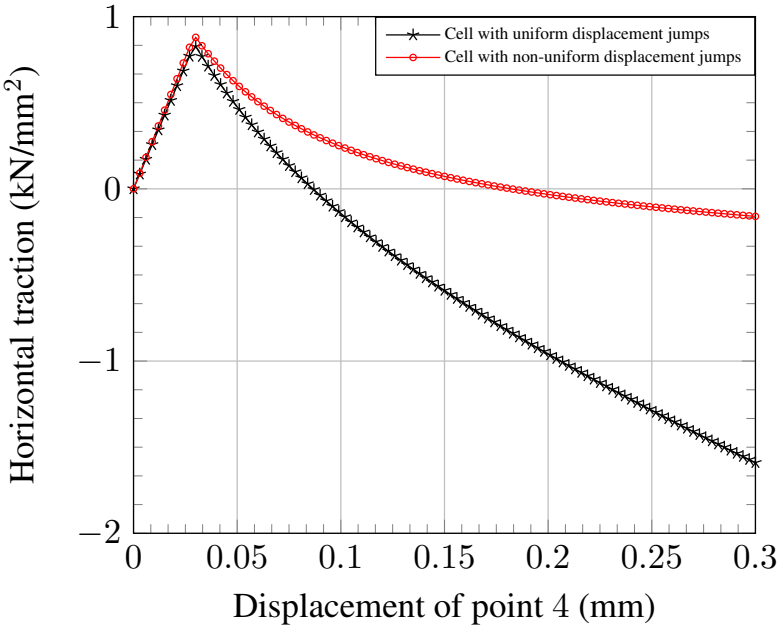


Figure 6. Example 1: Traction surface in collocation point 4

It can be seen by Fig. 6 that an elevated spurious negative traction is required in collocation point 4, when cells with uniform displacement jumps are used, to accomplish the displacement difference between points 5 and 4, while a more realistic traction curve is verified for the case with cell with non-uniform displacement jumps components.

Moreover, as depicted in Fig. 7, an adequate unloading branch was observed only when a cell with non-uniform displacement jumps components was used, while an accentuated stress locking behaviour was verified in the other case. It can be explained by the fact that the cell with only one collocation point is not able to capture rotational movements as the new cell here proposed. That is, a cell with uniform displacement jumps components can only capture translational rigid body motions between the

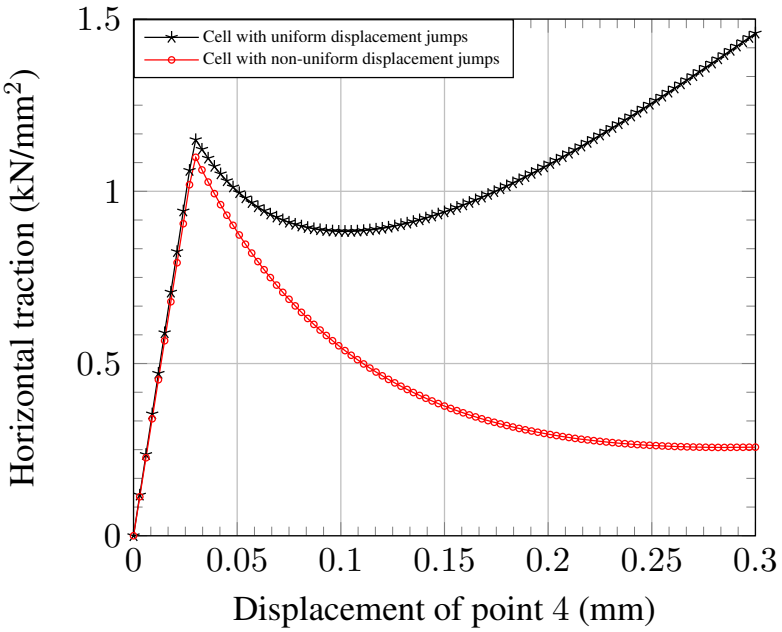


Figure 7. Example 1: Traction surface in collocation point 5

two portions of the cell. Thus, the cells with non-uniform displacement jumps components is more appropriate to be used.

### 7.2 Example 2: Four point bending

The second example analyzed is the four point bending test that was experimentally studied by Arrea and Ingraffea [52]. This problem is showed in Fig. 8, where the material properties are also presented.

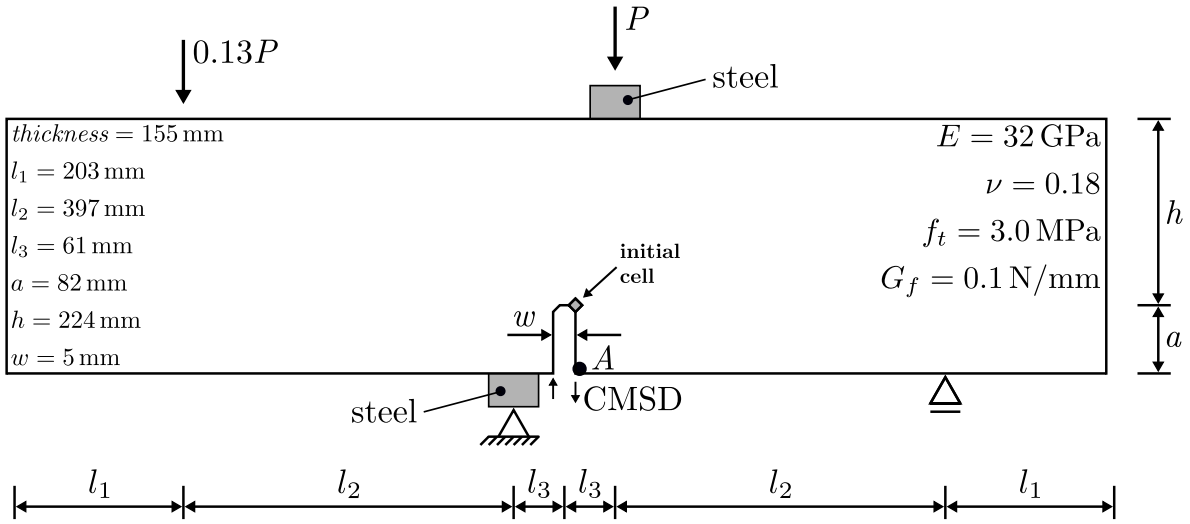


Figure 8. Example 2: Four point bending test

The boundary discretization was performed with 642 linear elements. To capture the beginning of the discontinuity line, a square cell with diagonal of 1.6 mm was previously introduced at the notch tip. In this cell the origin of the discontinuity segment was imposed at the midpoint of the side common to the notch boundary. The automatic cell generation algorithm was adopted with $\beta = 1.001$, but with cell growth being interrupted when the discontinuity segment exceeded 8.0 mm. In addition, 170 steps are considered in the non-linear analysis with its progression being controlled through the vertical displacement component of point $A$, highlighted in Fig. 8. In this way, the final mesh obtained is shown

in Fig. 9.

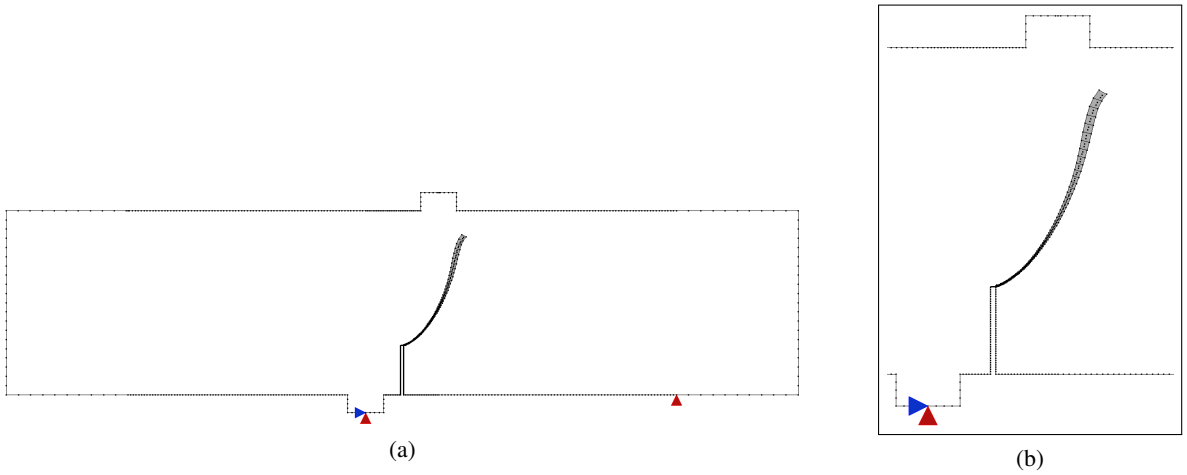


Figure 9. Example 2: (a) Total mesh, (b) Detail

The results for the applied load versus the relative vertical displacement between the two sides at the botton portion of the notch (*the crack mouth sliding displacement* - CMSD) is presented through the Fig. 10, again considering the analyses with cells with uniform and non-uniform displacement jumps components, plotted over the experimental envelopment results [52]. Beside this, for comparison purposes, the results obtained by Manzoli and Venturini [31] and Manzoli *et al.* [45] are also presented in this same figure. In these both works, triangular cells with embedded uniform displacement jumps (only one collocation point) were employed. In the firs one, an standard associative elastoplastic constitutive model with a tensile strength of 2.5 MPa were employed, while in the second, an isotropic damage model, similar to the one here employed, was adopted with $f_t = 3.5$ MPa. All the remaining physical properties follows the same values as presented in Fig. 8.

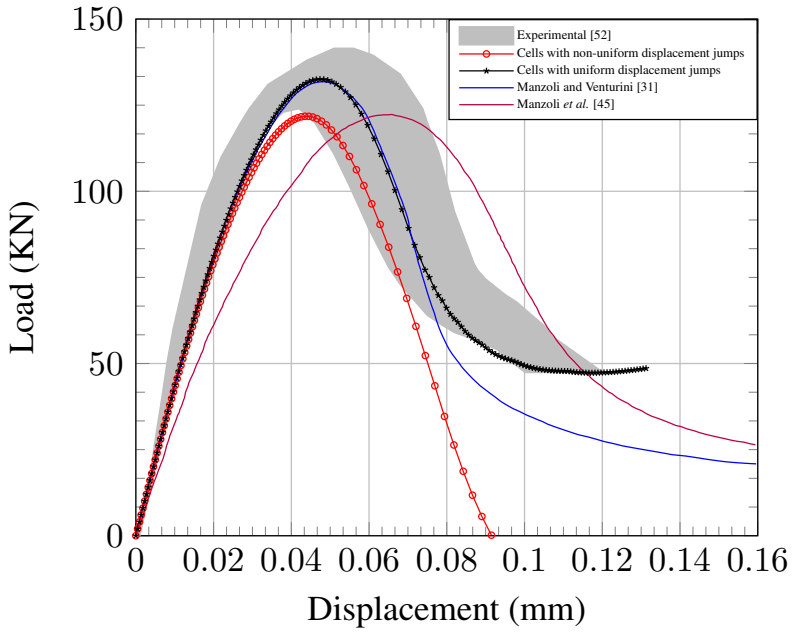


Figure 10. Example 2: Results for load *P* versus CMSD

It is possible to verify that all the three analyses using cells with embedded uniform displacement jumps presented the stress locking behaviour, preventing the total stress release associated to the final fracture of the structure. On the other hand, the complete unloading occurs for the analysis with the new type of cells here proposed.

## 8 Concluding remarks

Until the present moment, only uniform quadrilateral cells had been employed in crack propagation problems within the BEM. Thus, in the present work quadrilateral cells with non-uniform embedded discontinuity were developed. In numerical analysis, the implicit formulation of the boundary element method was considered together with the CSDA. Initially was analyzed a simple bending test and, subsequently, numerical simulations were performed with an automatic cell generation algorithm considering one classical problem whose experimental results are available in the literature. All analyses were performed with uniform and non-uniform cells in order to demonstrate the efficacy in the use of the cells developed here.

The results obtained for the simple bending test showed that uniform quadrilateral cells present the stress locking phenomenon, which, in turn, is greatly reduced with the use of non-constant quadrilateral cells. This phenomenon arises due to the inability of uniform quadrilateral cells to represent the relative rotational movement between their two parts inducing, in turn, an unrealistic stiffening in the structural response. That is, this type of cell is not able to completely relieve the stresses within it when requested in mixed-modes of fracture. Subsequently, in the example 2, the stress locking phenomenon was completely removed due to the continuous softening present in the curve (Load $\times$ CMSD - Fig. 10), until the end of the analysis. This event is not observed in analyses with uniform cells which, in turn, show a slight stiffening in this same curve in its final stage. Another important fact to be highlighted in this last example is the almost complete unloading of the structural response. That is, as the generated cells approach the top of the model, the collapse of the structure and the consequent complete unloading in curve (Load $\times$ CMSD) is expected, evidencing that the cells developed in this work are more consistent with the physical reality of the problem.

## Acknowledgements

The authors would like to acknowledge CNPq (National Council of Scientific and Technological Development), CAPES (Coordination of Improvement of Higher Education Personnel), FAPEMIG (Minas Gerais State Research Foundation) and PROPEEs/UFMG (Structure Engineering Graduate Program of the Federal University of Minas Gerais) for financial supports.

## References

[1] Inglis, C. E., 1913. The phenomena of rupture and flow in solids. *Philosophical Transactions of the Royal Society A*, vol. 55, pp. 219–241.

[2] Griffith, A. A., 1921. The phenomena of rupture and flow in solids. *Philosophical Transactions of the Royal Society A*, vol. 221, pp. 163–198.

[3] Paris, P., Gomez, M., & Anderson, W., 1961. A rational analytic theory of fatigue. *The Trend in Engineering*, vol. 13, pp. 9–14.

[4] Rice, J., 1968. A path independent integral and the approximate analysis of strain concentration by notches and cracks. *Journal of Applied Mechanics*, vol. 35, pp. 379–386.

[5] Shephard, M. S., Yehia, N. A. B., Burd, G. S., & Weidner, T. J., 1985. Computational strategies for nonlinear and fracture mechanics problems: automatic crack propagation tracking. *Computers & Structures*, vol. 20, pp. 211–223.

[6] Swenson, D. V. & Ingraffea, A. R., 1988. Modeling mixed-mode dynamic crack propagation using finite elements: Theoty and applications. *Computational Mechanics*, vol. 3, pp. 381–397.

[7] Portela, A., Aliabadi, M. H., & Rooke, D. P., 1992. The dual boundary element method: effective implementation for cracked problems. *International Journal for Numerical Methods in Engineering*, vol. 33, pp. 1269–1287.

[8] Hillerborg, A., Modeer, M., & Petersson, P. E., 1976. Analysis of crack formation and crack growth in concrete by means of fracture mechanics and finite elements. *Cement and Concrete Research*, vol. 6, pp. 773–782.

[9] Ingraffea, A. R. & Saouma, V., 1985. Numerical modeling of discrete crack propagation in reinforced and plain concrete. In Sih, G. C. & Tommaso, A. D., eds, *Fracture Mechanics of Concrete. Structural Application and Numerical Calculation* , pp. 171–225. Martinus Nijhoff, Dordrecht.

[10] Klisinski, M., Runesson, K., & Sture, S., 1991. Finite element with inner softening band. *Journal of Engineering Mechanics*, vol. 117, pp. 575–587.

[11] Dvorkin, E., Cuitino, A., & Gioia, G., 1990. Finite elements with displacement embedded localization lines insensitive to mesh sizes and distortions. *International Journal for Numerical Methods in Engineering*, vol. 30, pp. 541–564.

[12] Saleh, A. L. & Aliabadi, M. H., 1995. Crack growth analysis in concrete using boundary element method. *Engineering Fracture Mechanics*, vol. 51, pp. 533–545.

[13] Rashid, Y. R., 1968. Ultimate strenght analysis of prestressed concrete pressure vessels. *Nuclear Engineering and Design*, vol. 7, pp. 334–344.

[14] Cope, R. J., Rao, P. V., Clark, L. A., & Norris, P., 1980. Modelling of reinforced concrete behaviour for finite element analysis of bridgeslabs. In Taylor, C., Hinton, E., & Oden, D. R. J., eds, *Numerical Methods for Nonlinear Problems 1* , pp. 457–470. Pineridge Press, Swansea. Cited by Chaves [53].

[15] Jirásek, M. & Zimmermann, T., 1998. Analysis of rotating crack model. *Journal of Engineering Mechanics - ASCE*, vol. 124, pp. 842–851.

[16] Bažant, Z. P. & Oh, B. H., 1983. Crack band theory for fracture of concrete. *Matériaux et Constructions*, vol. 16, pp. 155–177.

[17] Rots, J. G., Nauta, P., Kusters, G. M. A., & Blaauwendraad, J., 1985. Smeared crack approach and fracture localization in concrete. *HERON*, vol. 30, pp. 1–48.

[18] Muhlhaus, H.-B. & Vadoulakis, I., 1987. The thickness of shear bands in granular materials. *Geotechnique*, vol. 37, pp. 271–283.

[19] de Borst, R., 1991. Simulation of strain localization: A reappraisal of the Cosserat continuum. *Engineering Computations*, vol. 8, pp. 317–332.

[20] de Borst, R. & Muhlhaus, H.-B., 1992. Gradient-dependent plasticity: Formulation and algorithmic aspects. *International Journal for Numerical Methods in Engineering*, vol. 35, pp. 521–539.

[21] Simo, J. C., Oliver, J., & Armero, F., 1993. An analysis of strong discontinuities induced by strain-softening in rate-independent inelastic solids. *Computational Mechanics*, vol. 12, pp. 277–296.

[22] Simo, J. C. & Oliver, J., 1994. Strong discontinuity analysis in solid mechanics using boundary element method. In Bažant, Z. P., Bittnar, Jirásek, M., & Mazars, J., eds, *Fracture and damage in quasibrittle structures: experiment, modelling and computer analysis*, pp. 25–39.

[23] Oliver, J., 1995. Continuum modelling of strong discontinuities in solid mechanics using damage models. *Computational Mechanics*, vol. 17, pp. 49–61.

[24] Oliver, J., 1996a. Modelling strong discontinuities in solid mechanics via strain softening constitutive equations. Part 1: Fundamentals. *International Journal for Numerical Methods in Engineering*, vol. 39, pp. 3575–3600.

[25] Oliver, J., 1996b. Modelling strong discontinuities in solid mechanics via strain softening constitutive equations. Part 2: Numerical simulation. *International Journal for Numerical Methods in Engineering*, vol. 39, pp. 3601–3623.

[26] Manzoli, O., Oliver, J., & Cervera, M., 1998. Localización de deformación: Análisis y simulación numérica de discontinuidades en mecánica de sólidos. Centro Internacional de Métodos Numéricos en Ingeniería (CIMNE). Monografía n. 44. Barcelona.

[27] Oliver, J., Cervera, M., & Manzoli, O., 1998. On the use of strain-softening models for the simulation of strong discontinuities in solids. In de Borst, R. & van der Giessen, E., eds, *Material instabilities in solids* , chapter 8, pp. 107–123. John Wiley & Sons, Chichester.

[28] Oliver, J., Cervera, M., & Manzoli, O., 1999. Strong discontinuities and continuum plasticity models: the strong discontinuity approach. *International Journal of Plasticity*, vol. 15, pp. 319–351.

[29] Oliver, J., 2000. On the discrete constitutive models induced by strong discontinuity kinematics and continuum constitutive equations. *International Journal of Solids and Structures*, vol. 37, pp. 7207–7229.

[30] Oliver, J., Huespe, A. E., Pulido, M. D. G., & Chaves, E., 2002. From continuum mechanics to fracture mechanics: the strong discontinuity approach. *Engineering Fracture Mechanics*, vol. 69, pp. 113–136.

[31] Manzoli, O. L. & Venturini, W. S., 2007. An implicit BEM formulation to model strong discontinuities. *Computational Mechanics*, vol. 40, pp. 901–909.

[32] Peixoto, R. G., Ribeiro, G. O., Pitangueira, R. L. S., & Penna, S. S., 2017. The strong discontinuity approach as a limit case of strain localization in the implicit bem formulation. *Engineering Analysis with Boundary Elements*, vol. 80, pp. 127–141.

[33] Peixoto, R. G., Ribeiro, G. O., & Pitangueira, R. L. S., 2018. A boundary element method formulation for quasi-brittle material fracture analysis using the continuum strong discontinuity approach. *Engineering Fracture Mechanics*, vol. 202, pp. 47–74.

[34] Kim, J. & Armero, F., 2017. Three-dimensional finite elements with embedded strong discontinuities for the analysis of solids at failure in the fnite deformation range. *Computer Methods in Applied Mechanics and Engineering*, vol. 317, pp. 890–926.

[35] Armero, F., 2012. Strong discontinuities in antiplane/torsional problems of computational failure mechanics. *International Journal of Fracture*, vol. 178, pp. 3–32.

[36] Ortiz, M., Leroy, Y., & Needleman, A., 1987. A finite element method for localized failure analysis. *Computer Methods in Applied Mechanics and Engineering*, vol. 61, pp. 189–214.

[37] Runesson, K., Ottosen, N. S., & Perić, D., 1991. Discontinuous bifurcations of elastic-plastic solutions at plane stress and plane strain. *International Journal of Plasticity*, vol. 7, pp. 99–121.

[38] van der Giessen, E. & de Borst, R., 1998. Introduction to material instabilities in solids. In de Borst, R. & van der Giessen, E., eds, *Material instabilities in solids*, chapter 1. John Wiley & Sons, Chichester.

[39] Oliver, J., Huespe, A. E., & Samaniego, E., 2003. A study on finite elements for capturing strong discontinuities. *International Journal for Numerical Methods in Engineering*, vol. 56, pp. 2135–2161.

[40] Manzoli, O. L. & Shing, P. B., 2006. A general technique to embed non-uniform discontinuities into standard solid finite elements. *Computers and Structures*, vol. 84, pp. 742–757.

[41] Oliver, J., Huespe, A. E., & Sánchez, P. J., 2006a. A comparative study on finite elements for

capturing strong discontinuities: E-FEM vs X-FEM. *Computer Methods in Applied Mechanics and Engineering*, vol. 195, pp. 4732–4752.

[42] Belytschko, T., Moës, N., Usui, S., & Parimi, C., 2001. Arbitrary discontinuities in finite elements. *International Journal for Numerical Methods in Engineering*, vol. 50, pp. 993–1013.

[43] Wells, G. N. & Sluys, L. J., 2001. A new method for modelling cohesive cracks using finite elements. *International Journal for Numerical Methods in Engineering*, vol. 50, pp. 2667–2682.

[44] Mariani, S. & Perego, U., 2003. Extended finite element method for quasi-brittle fracture. *International Journal for Numerical Methods in Engineering*, vol. 58, pp. 103–126.

[45] Manzoli, O. L., Pedrini, R. A., & Venturini, W. S., 2009. Strong discontinuity analysis in solid mechanics using boundary element method. In Spountzakis, E. J. & Aliabadi, M. H., eds, *Advances in Boundary Element Techniques X*, pp. 323–329, Atenas, Grécia.

[46] Lachat, J. C. & Watson, J. O., 1976. Effective numerical treatment of boundary integral equations - a formulation for three dimensional elastostatics. *International Journal for Numerical Methods in Engineering*, vol. 10, pp. 991–1005.

[47] Gao, X.-W. & Davies, T. G., 2000. An effective boundary element algorithm for 2D and 3D elastoplastic problems. *International Journal of Solids and Structures*, vol. 37, pp. 4987–5008.

[48] Peixoto, R. G., Anacleto, F. E. S., Ribeiro, G. O., Pitangueira, R. L. S., & Penna, S. S., 2016. A solution strategy for non-linear implicit BEM formulation using a unified constitutive modelling framework. *Engineering Analysis with Boundary Elements*, vol. 64, pp. 295–310.

[49] Oliver, J., Huespe, A. E., Blanco, S., & Linero, D. L., 2006b. Stability and robustness issues in numerical modeling of material failure with the strong discontinuity approach. *Computer Methods in Applied Mechanics and Engineering*, vol. 195, pp. 7093–7114.

[50] Ben-Israel, A. & Greville, T. N. E., 2003. Existence and construction of generalized inverses. In Borwein, J. & Borwein, P., eds, *Generalized inverses: Theory and applications* , pp. 40–51. Springer, New York.

[51] Mendonça, T. S., Peixoto, R. G., , & Ribeiro, G. O., 2018. Crack propagation using the continuum strong discontinuity approach by the bem: some numerical remarks. *Journal of the Brazilian Society of Mechanical Sciences and Engineering*, vol. 40, pp. 520.

[52] Arrea, M. & Ingraffea, A. R., 1982. Mixed-mode crack propagation in mortar and concrete. Technical report, 81-13, Department of Structural Engineering, Cornell University, Ithaca, USA.

[53] Chaves, E. A., 2003. *A new approach to the analysis and simulation of strain softening in solids*. PhD thesis, Universitat Politécnica de Catalunya, Barcelona.